

# Fabrication and Electric Field Dependent Transport Measurements of Mesoscopic Graphite Devices

Yuanbo Zhang, Joshua P. Small, William V. Pontius, and Philip Kim  
*Department of Physics and the Columbia Nanoscale Science and Engineering Center,  
 Columbia University, New York, New York 10027*

We have developed a unique micromechanical method to extract extremely thin graphite samples. Graphite crystallites with thicknesses ranging from 10 - 100 nm and lateral size  $\sim 2 \mu\text{m}$  are extracted from bulk. Mesoscopic graphite devices are fabricated from these samples for electric field dependent conductance measurements. Strong conductance modulation as a function of gate voltage is observed in the thinner crystallite devices. The temperature dependent resistivity measurements show more boundary scattering contribution in the thinner graphite samples.

The recent focus of research in graphitic materials, such as fullerenes [1] and carbon nanotubes [1, 2] has renewed interest in electronic transport in graphene, a single atomic layer of graphite. While graphite is a semimetal with strong electron and hole compensation, graphene is expected to be a zero-gap semiconductor with a vanishing density of states at the charge neutral point. Electrical transport in thin graphite crystals composed of only a few graphene layers is of particular interest in elucidating the evolution of electronic structure from bulk single crystals to two-dimensional planar systems. Experimental work to synthesize very thin graphitic layers directly on top of a substrate [3] or to extract using chemical [4], or mechanical [5, 6] pathways has been demonstrated to produce graphitic samples with thicknesses ranging from 1 - 100 nm. Systematic transport measurements have been carried out on mesoscopic graphitic disks [7] and cleaved bulk crystals [8] with sample thicknesses approaching  $\sim 20$  nm, exhibiting persisting bulk graphite properties at these length scales. However, electric field dependent charge transport has not been measured, due to the fact that the size of the samples and the geometry of the devices are inadequate for such a measurement.

In this letter, we present a unique method to extract mesoscopic graphite crystallites, with thicknesses ranging from 10 - 100 nm, from bulk highly oriented pyrolytic graphite (HOPG) using micromechanical manipulation and microfabrication techniques. Mesoscopic devices consisting of these graphite crystallites are fabricated for electrical transport measurement. A degenerately doped Si substrate serves as a back gate, allowing us to probe the electrical properties as a function of charge concentration. Electrical conductance of these mesoscopic graphite devices exhibits significant gate voltage dependence. From the temperature dependent resistivity measurements in these samples, we deduce the scattering rate of mesoscopic graphite of varying thicknesses.

The graphite samples used in this study are extracted from HOPG (Grade-1, Structure Probe, Inc.). Following a similar technique demonstrated in [6], arrays of graphite micro-pillars ( $\sim 2 \times 2 \times 5 \mu\text{m}^3$ ) are fabricated on the HOPG surface using micropatterning followed by

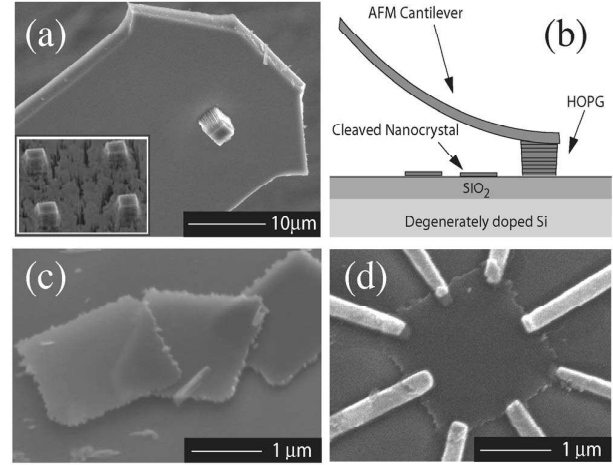


FIG. 1: (a) scanning electron microscope image of an HOPG crystallite mounted on a microcantilever. Inset: Bulk HOPG surface patterned by masked anisotropic oxygen plasma etching. (b) Schematic drawing of the micro-cleaving process. (c) Thin graphite samples cleaved onto the SiO<sub>2</sub>/Si substrate. (d) A typical mesoscopic device fabricated from a cleaved graphite sample.

masked anisotropic oxygen plasma etching (Fig. 1(a) inset). Once the array is formed, an individual block of the pillar is removed from the surface using a precision micro-manipulator under a high resolution optical microscope. The detached graphite block is then transferred to a micro-machined silicon cantilever (MikroMasch), where it is glued down by a small amount of ultra violet sensitive epoxy (Fig. 1(a)).

In the next step, we use the mounted graphite block on the cantilever as the tip of an atomic force microscope (AFM) in order to transfer thin graphite samples onto a SiO<sub>2</sub>/Si substrate for subsequent device fabrication. By operating the AFM (Nanoscope IIIa Multimode, Digital Instruments) in contact mode with load on the graphite mounted cantilever, very thin layers of HOPG are sheared off onto the substrate (Fig.1(b)). This microscopic cleaving process can be controlled by tuning the loading normal force between the cantilever and the substrate. The van der Waals binding energy between

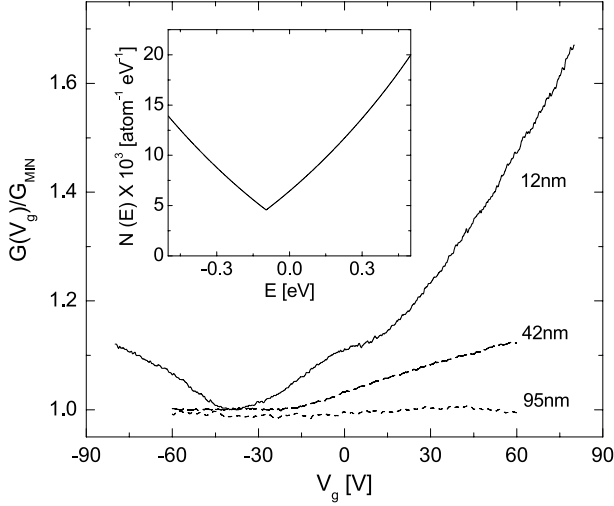


FIG. 2: Normalized conductance measured in samples of varying thickness as a function of gate voltage at  $T = 1.7$  K. Inset: Calculated density of states for bulk graphite [10].

the graphene layers in graphite is  $\sim 2$  eV nm $^{-2}$  [9]. Assuming the graphite-substrate friction coefficient is  $\sim 1$ , the required normal force to cleave off a  $1 \mu\text{m}^2$  graphite sheet from the top of the crystallite is  $\sim 300$  nN. A normal force in the range of 10 - 2000 nN can be easily managed by commercially available silicon cantilevers. In our experiment, by fine tuning the normal force, square graphite crystallites with lateral size  $\sim 2 \mu\text{m}$  and thicknesses ranging from 10 - 100 nm are easily obtained using this process (Fig.1(c)). Once the graphite samples are cleaved onto a substrate with predefined alignment marks, AFM images are acquired for measuring the height of the cleaved crystallites and registering the position for device design. The Cr/Au (1 nm/30 - 180 nm) electrodes are then fabricated by electron beam lithography. Typically, multiple contacts are fabricated around the square graphite crystallites allowing us to perform conductivity measurements using van der Pauw method. In addition, a degenerately doped silicon substrate is used as a gate electrode with 500 nm of thermally grown silicon oxide acting as the gate dielectric.

Fig. 2 shows the conductance,  $G$ , versus the gate voltage,  $V_g$ , at 1.7 K for samples with varying thicknesses. The curves are normalized with their minimum values  $G_{min} = G(V_g^{min})$ , where  $V_g^{min} \approx -40$  V. As  $\Delta V_g = V_g - V_g^{min}$  moves away from zero,  $G(V_g)$  increases, increasing more rapidly for thinner samples. Specifically, at  $\Delta V_g = 100$  V,  $G/G_{min}$  is 1.47 and 1.12 for the samples with thickness 12 and 42 nm respectively, while no appreciable change is observed in the 95 nm sample. This observation implies a larger electric field effect in thinner samples, as expected.

Considering the electrostatic coupling between the samples and the gate, the observed behavior of  $G(V_g)$  at low temperatures can be understood quantitatively as discussed below. When the gate voltage is applied, the

electrostatic potential at the surface of the sample rises to  $\phi_0$ , and a charge density  $n_{ind}(z)$  is induced in the sample, where  $z$  is measured from the interface of the sample and the substrate. Following the Thomas-Fermi approximation [11], the electrostatic potential in the sample is given by  $\phi(z) = \phi_0 e^{-z/\lambda_s}$ , where  $\phi_0$  is a constant (determined below) and  $\lambda_s$  is the screening length.  $\lambda_s$  can be inferred from  $\phi/\lambda_s^2 = -en_{ind}/\epsilon_0$ , where  $e$  and  $\epsilon_0$  are the electron charge and vacuum permittivity, respectively. The total amount of induced charge in the sample with thickness  $d$  is related to the capacitance of the sample to gate per unit area,  $C_g$ , by  $C_g(V_g - \phi_0) = -\int_0^d en_{ind}(z)dz$ . Evaluating this integral, we obtain  $\phi_0 = V_g/(1 + C_Q/C_g)$ , where the sample dependent quantum capacitance per unit area  $C_Q = \epsilon_0(1 - e^{-d/\lambda_s})/\lambda_s$ .

In order to estimate the enhanced conductance in the presence of an induced charge density gradient, we use Einstein's relation for local conductivity  $\sigma(z) = e^2 N(E_F) D(E_F)$ , where  $N(E_F)$  and  $D(E_F)$  are the density of states and the electron diffusion coefficient at Fermi energy  $E_F$ , respectively. In graphite both of these quantities are sensitive to the change of  $E_F$ , thus it should be accounted for in the determination of local conductivity in the presence of an electric field. Assuming our samples retain the band structure of bulk graphite, the functional form of  $N(\epsilon)$  can be obtained from graphite band structure calculations (Fig. 2 inset) [10]. Here  $\epsilon$  is measured from the charge neutral point, where  $N(\epsilon)$  has its minimum value. For the energy range  $|\epsilon| < 300$  meV, we can approximate  $N(\epsilon) \approx N_0(1 + \beta|\epsilon|)$ , where  $N_0 = 5.2 \times 10^{20} \text{ cm}^{-3} \text{ eV}^{-1}$  and  $\beta = 4.8 \text{ eV}^{-1}$ . A further assumption is required to estimate  $D(E_F)$  in the presence of an electrostatic potential. Here, we adopt the simple two band (STB) model [12], which has been successful in explaining electron transport in bulk graphite [13]. Assuming the scattering time,  $\tau$ , and effective mass of carriers are relatively insensitive to change of  $E_F$ , the STB model yields  $D(\epsilon) \propto v_F^2 \tau \propto |\epsilon + E_0|$ , where  $v_F$  is the Fermi velocity and  $E_0$  half the band overlap between the electron and hole bands. With these assumptions, the normalized conductance of the sample is given by

$$G(V_g)/G_{min} = \int_0^d dz N(\epsilon) |\epsilon + E_0| / N_0 E_0 d \quad (1)$$

where  $\epsilon(z) = -e\phi_0 e^{-z/\lambda_s}$ . In order to compare this equation to our experimental observations, the values of  $\lambda_s$  and  $E_0$  are needed. We use the following values from the literature:  $\lambda_s = 0.4$  nm [14] and  $E_0 = 0.015$  eV [15]. Employing these values, we estimate  $C_g$  by comparing Eq. 1 to the experimentally observed values. The corresponding  $C_g$  are  $30 \text{ aF}\mu\text{m}^{-2}$  and  $27 \text{ aF}\mu\text{m}^{-2}$  for 12 nm and 42 nm thick graphite devices, respectively. These values are in reasonable agreement with the value of  $C_g$  obtained by considering the device geometry.

We now turn our attention to the temperature dependence of the electrical conductance in samples of varying thickness. Fig. 3 shows the resistivity normalized to

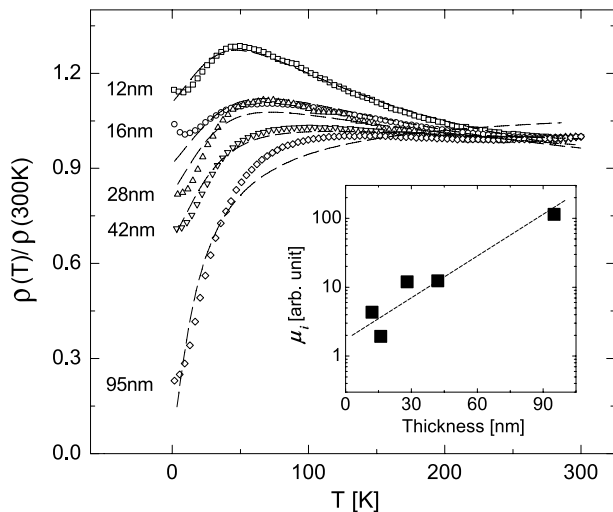


FIG. 3: Resistivity (normalized to its 300 K value) as a function of temperature,  $T$ , for  $d$  ranging from 12 - 95 nm at  $V_g = 0$ . While the thicker samples show a metallic behavior ( $d\rho/dT > 0$ ), thinner samples develop a more complicated behavior in  $T$ . This behavior can be understood by considering two competing factors as the temperature varies. Assuming the mobility,  $\mu$ , is similar for the compensating electrons and holes in the samples, the sample resistivity is given by  $\rho = 1/(|e|\mu n)$ , with the total charge carrier density  $n = n_e + n_h$ , where  $n_e$  and  $n_h$  are the carrier densities of electrons and holes, respectively. In the STB model, for completely compensated samples (i.e.,

its room temperature value,  $\rho(T)/\rho(300K)$ , as a function of temperature,  $T$ , for  $d$  ranging from 12 - 95 nm at  $V_g = 0$ . While the thicker samples show a metallic behavior ( $d\rho/dT > 0$ ), thinner samples develop a more complicated behavior in  $T$ . This behavior can be understood by considering two competing factors as the temperature varies. Assuming the mobility,  $\mu$ , is similar for the compensating electrons and holes in the samples, the sample resistivity is given by  $\rho = 1/(|e|\mu n)$ , with the total charge carrier density  $n = n_e + n_h$ , where  $n_e$  and  $n_h$  are the carrier densities of electrons and holes, respectively. In the STB model, for completely compensated samples (i.e.,

$\Delta V_g = 0$ ),  $n/2 = n_e = n_h = C_0 k_B T \ln(1 + \exp \frac{E_0}{k_B T})$ , where  $k_B$  is Boltzmann constant and  $C_0$  a constant independent of  $T$  [12]. We further assume that the mobility can be expressed as  $\mu^{-1} = \mu_i^{-1} + A_0 T$ , where  $\mu_i^{-1}$  is the contribution from static scattering centers and  $A_0$  is a constant depending on electron-phonon scattering in graphite. Then, as  $T$  increases,  $\mu$  decreases due to increasing electron-phonon scattering, while  $n$  increases rapidly due to the thermal excitation of charge carriers around  $E_F$ . Using  $E_0$  and  $A_0 \mu_i$  as fitting parameters, this model fits well with our experimental observations over a large temperature range and samples with varying thicknesses (broken lines in Fig. 3). As a result of the fit, we obtain  $E_0 \sim 10 - 20$  meV, which is in reasonable agreement with the values found in the literature [15]. In addition, we obtain  $A_0 \mu_i$  from the same fit. Assuming  $A_0$  is similar for all measured samples, the  $\mu_i$  for different samples can be compared. The inset of Fig. 3 shows decreasing  $\mu_i$  as sample thickness is reduced. An increasing contribution of boundary scattering at the sample surfaces can explain this behavior. We note, however, that the reduction of  $\mu_i$  seems to saturate as  $d \rightarrow 0$ . In addition, our recent galvanomagnetic measurements [16] in these samples showed that the quantum oscillations in electron transport can be readily observed at high magnetic fields. Both observations suggest that the quality of the sample has not degraded after our micromechanical extraction from the bulk.

We thank Y. Wu for help in sample processing, V. Oganessian and P. McEuen for helpful discussions. This work is supported primarily by the Nanoscale Science and Engineering Initiative of the National Science Foundation under NSF Award Number CHE-0117752 and by the New York State Office of Science, Technology, and Academic Research (NYSTAR).

- 
- [1] M. S. Dresselhaus, G. Dresselhaus, and P. C. Eklund, *Science of Fullerenes and Carbon Nanotubes* (Academic, 1996).
  - [2] M. S. Dresselhaus, G. Dresselhaus, and Ph. Avouris eds., *Carbon Nanotubes* (Springer-Verlag, 2001).
  - [3] H. Itoh, T. Ichinose, C. Oshima and T. Ichinokawa, *Surf. Sci. Lett.* **254**, L437 (1991); T. A. Land, T. Michely, R. J. Behm, J. C. Hemminger, and G. Comsma, *Surf. Sci.* **264**, 261 (1992).
  - [4] L. M. Viculis, J. J. Jack, and R. B. Kaner, *Science* **299**, 1361 (2003).
  - [5] T. W. Ebbensen and H. Hiura, *Adv. Mater.* **7**, 582 (1995).
  - [6] X. Lu, H. Huang, N. Nemchuk, and R. Ruoff, *Appl. Phys. Lett.* **75**, 193 (1999); X. Lu, M. Yu, H. Huang, and R. Ruoff, *Nanotechnology* **10**, 269 (1999).
  - [7] E. Dujardin, T. Thio, H. Lezec, and T. W. Ebbesen, *Appl. Phys. Lett.* **79**, 2474 (2001).
  - [8] Y. Ohashi, T. Hironaka, T. Kubo, and K. Shiiki, *Tanso* **1997**, 235 (1997); Y. Ohashi, T. Hironaka, T. Kubo, and K. Shiiki, *Tanso* **2000**, 410 (2000).
  - [9] L. A. Girifalco and R. A. Lad, *J. Chem. Phys.* **25**, 693 (1956).
  - [10] J. W. McClure, *Phys. Rev.* **3**, 612 (1957).
  - [11] N. W. Ashcroft and N. D. Mermin, *Solid State Physics* (Harcourt College, 1976).
  - [12] For an extensive summary see, for example, B. T. Kelly *Physics of Graphite* (Applied Science, 1981), pp285.
  - [13] For most recent experiments, see, for example, X. Du, S. Tsai, D. Maslov, and A. F. Hebard, *cond-mat/0404725* (2004).
  - [14] P. R. Visscher and L. M. Falicov, *Phys. Rev. B* **3**, 2541 (1971).
  - [15] N. B. Brandt, S. M. Chudinov, and Y. G. Ponomarev, *Semimetals 1: Graphite and its compounds* (North-Holland, 1988).
  - [16] Y. Zhang, J. P. Small, M. Amori, and P. Kim, submitted for publication.